Soft Matter

PAPER

Structural behaviour differences in low methoxy pectin solutions in the presence of divalent cations (Ca^{2+} and Zn^{2+}): a process driven by the binding mechanism of the cation with the galacturonate unit†

Ali Assifaoui,*[ad] Adrien Lerbret,*[a] Huynh T. D. Uyen,[a] Fabrice Neiers,[b] Odile Chambin,[ad] Camille Loupiac[ac] and Fabrice Cousin[c]

In this paper, we compare the interactions between low methoxy pectin (LMP) and either Ca^{2+} or Zn^{2+} in semi-dilute solutions. Intrinsic viscosity and turbidity measurements reveal that pectin–calcium solutions are more viscous, but yet less turbid, than pectin–zinc ones. To get a molecular understanding of the origin of this rather unexpected behavior, we further performed isothermal titration calorimetry, small angle neutron scattering experiments, as well as molecular dynamics simulations. Our results suggest that calcium cations induce the formation of a more homogeneous network of pectin than zinc cations do. The molecular dynamics simulations indicate that this difference could originate from the way the two cations bind to the galacturonate unit (Gal), the main component of LMP: zinc interacts with both carboxylate and hydroxyl groups of Gal, in a similar way to that described in the so-called egg-box model, whereas calcium only interacts with carboxylate groups. This different binding behavior seems to arise from the stronger interaction of water molecules with zinc than with calcium. Accordingly, galacturonate chains are more loosely associated with each other in the presence of Ca^{2+} than with Zn^{2+}. This may improve their ability to form a gel, not only by dimerization, but also by the formation of point-like cross-links. Overall, our results show that zinc binds less easily to pectin than calcium does.

Introduction

Pectin is an anionic polysaccharide present in the cell wall of various plants, which has been widely used in food and pharmaceutical industries as a gelling, stabilizing and/or encapsulating agent. It is well known that gelation occurs when pectin is in contact with divalent cations.[1–4] This gelling property has made pectin a suitable delivery system to escort active compounds from the mouth to the colon.[5] It may be used to create various dosage forms with specific drug release profiles. Pectin is composed of long sequences of partially methyl-esterified (1–4)-linked α-D-galacturonic residues (known as

'smooth regions' or homogalacturonan), interrupted by defects of other neutral sugars such as D-xylose, D-glucose, L-rhamnose, L-arabinose and D-galactose (known as the non-gelling 'hairy' region).[6] Depending on the number of methyl ester groups (referred to as the degree of esterification, DE) pectin is classified as high methoxy pectin (HMP) (DE > 50%) or low methoxy pectin (LMP) (DE < 50%). The affinity of LMP towards divalent cations increases when decreasing DE or ionic strength, and when increasing the polymer concentration. Moreover, the distribution of the galacturonate residues (deprotonated form of galacturonic acid, see Fig. S1 in the ESI†) has a strong effect on the polymer's ability to bind various divalent cations.

Considerable attention has been paid to the study of the binding mechanisms of pectin chains to explain the pectin's affinity towards divalent cations such as Ca^{2+}. The association between LMP chains is due to three types of interactions: (i) hydrophobic association between methoxyl ester groups, (ii) hydrogen bonds between galacturonic acid and/or hydroxyl groups, and (iii) ionic interactions between galacturonate unit (Gal) groups mediated by Ca^{2+}-bridges.[7] Previous studies on calcium–pectin binding have shown that a minimal number of consecutive Gal groups, estimated to lie between 8 and 15, is required to form a stable cross-link structure between two

[a]UMR PAM, AgroSup Dijon - Université de Bourgogne, Dijon, France. E-mail: ali.assifaoui@u-bourgogne.fr; adrien.lerbret@u-bourgogne.fr

[b]CSGA, INRA-CNRS-Université de Bourgogne, Bd Sully, Dijon, France

[c]Laboratoire Léon Brillouin, CEA-Saclay, Gif-sur-Yvette, France

[d]Department of Pharmaceutical Technology, School of Pharmacy, Université de Bourgogne, Bd Jeanne d'Arc, Dijon, France

† Electronic supplementary information (ESI) available: Details of all the MD simulations performed; schematic structure of the Gal unit; potentials of mean force for the interaction of cations with Gal and associated representative configurations; figure and movies on the binding of Gal chains in the presence of Ca^{2+} and Zn^{2+}. See DOI: 10.1039/c4sm01839g

chains in the presence of calcium (*dimerization*).[8–10] Chain association occurs by dimerization, which corresponds to long chain segments where the cations are sandwiched within the dimer on specific sites along each of the inner surfaces. This is commonly referred to as the egg-box model, originally proposed for the calcium–alginate complex by Grant *et al.*[11] Because pectin and alginate share a strongly similar structure (polygalacturonate and polyguluronate are nearly mirror images in structure) and binding behavior toward calcium, the egg-box model has been transposed to describe calcium–pectin binding, but its validity has not been established. At molecular scale, this model considers that calcium is coordinated to 10 oxygen atoms from two guluronate chains.[11] These include two hydroxyl oxygens (O2 and O3), two ether oxygens (O1/O4 and O5) and one carboxyl oxygen (O6) (see Fig. S1 in the ESI† for atom names) for each chain. But, this model was questioned by Braccini and Pérez, who argued that the coordination of calcium in calcium–carbohydrate complexes is usually between 7 and 9.[12] Indeed, among all these oxygens, only four (O6 and O2/O3 from two opposite carboxyl and hydroxyl groups) strongly interact with calcium (distance < 3 Å) in a monodentate coordination.

Fang *et al.*[13] showed by isothermal titration calorimetry that the binding of LMP to calcium is described by a two-step process: in step I (molar ratio R (Ca^{2+}/Gal) $\leq$ 0.25), the binding heat decreased, which was attributed to *monocomplexation* (binding of calcium with one Gal chain). In step II ($R > 0.25$), the binding heat increased, thereby indicating the formation of eggbox dimers (dimerization) through the pairing of monocomplexes.[13] They also suggested that the dimerization of pectin chains takes place progressively upon addition of calcium.

Pectin can be used as a drug delivery device to a specific site for targeted release. As LM pectins gel in the presence of divalent cations, they can be used to prepare pectinate gel beads containing a drug to be delivered. The drug release profile and encapsulation efficiency of pectin-based dosage forms (dry beads) strongly depend on the nature of the divalent cations used. For example, Assifaoui *et al.* showed that the drug release in pectin-based dosage forms prepared with calcium is faster than in those prepared with zinc.[14,15] This difference was explained by the higher swelling of the dosage forms when calcium was used instead of zinc. Further Fourier-transform infrared analysis showed that the bands of functional groups present in pectin are not affected when the content of zinc is increased, conversely to what happens in the presence of Ca^{2+}, indicating that zinc interacts with pectin to a lesser extent than calcium does.[16] It is likely that the properties of these beads are reminiscent from the structure of the gels formed in aqueous solution before being dried. Therefore, in the present paper, we investigate the differences between the binding processes of two divalent cations (Ca^{2+} and Zn^{2+}) to low methoxy pectin in semidilute solution at the molecular scale and describe how such a difference affects the properties of the solutions. The interactions of the divalent cations with LMP were studied by isothermal titration calorimetry (ITC) and by molecular dynamics (MD) simulations. Furthermore, the structures formed by the LMP in presence of cations at different length

scales were investigated by coupling small angle neutron scattering (SANS), turbidity and viscosity measurements. Thanks to the combination of results from these different techniques, we finally propose a mechanism for the binding of calcium and zinc with LMP.

Materials and methods

Materials

The pectin used (Unipectin OF 300 C) is a low methoxylated citrus pectin from Cargill France with 81% of galacturonic acid content, and a degree of esterification (DE) of 30%. The intrinsic viscosity, [η], at 30 °C in acetate buffer (pH = 5.3) is equal to 0.23 L g^{-1}. Note that the pH studied is 2 pH-unit above the pK_a of pectin's carboxylic groups to deprotonate them and obtain only galacturonate (Gal). Before use, we purified pectin using the alcohol-precipitation procedure.[17] Acetic acid, sodium acetate, calcium chloride dihydrate, zinc chloride and sodium perchlorate were of analytical grade (Sigma-Aldrich) and were used as received.

Methods

Sample preparation. We dispersed the pectin powder in an acetate buffer (pH = 5.3) composed of acetic acid (20 mM) and sodium acetate (80 mM). The final concentration of pectin was 1 g L^{-1}. Taking into account the Gal content (81%) and the DE (30%) of the pectin, the concentration of the Gal unit was equal to 0.56 g L^{-1}. This corresponds to a 2.90 mM concentration of Gal, since the molecular weight of the Gal unit is 194 g mol^{-1}. Calcium and zinc mother stock solutions were also prepared in the same acetate buffer and their concentrations were equal to 24 mM. For all experiments, different amounts of divalent cations were added to the pectin solution to obtain various molar ratios, R, (R = cation/Gal).

Turbidity measurements. We measured the turbidity of pectin solutions (2.90 mM of Gal) at different calcium and zinc concentrations in acetate buffer (pH = 5.3) using an ultraviolet-visible (UV) spectrophotometer (Biochrom Libra, France) at a wavelength of 500 nm and at room temperature. Samples were analyzed in a quartz cuvette with a cell path length of 1 cm. We introduced 2 mL of the pectin solution into the cell and then we added various amounts of calcium or zinc solution (24 mM) to obtain various cation/Gal ratios. The mixture was then stirred and the transmittance was recorded. All the measurements were done at least in triplicate. We determined turbidity, τ (cm^{-1}), from the following equation (eqn (1)):

$$\tau = \left(-\frac{1}{L}\right)\ln\left(\frac{I_t}{I_0}\right) \tag{1}$$

where L is the optical path length (=1 cm), and I_t and I_0 are the transmitted and incident light intensities, respectively.

Isothermal titration calorimetry. We used an isothermal titration calorimeter (VP-ITC microcalorimeter from GE Healthcare) to measure the enthalpies for the binding of Ca^{2+} or Zn^{2+} to pectin at 25 °C. Before each experiment, all solutions were degassed for 15 minutes. A volume of 5 μL of 24 mM of

divalent cation solution ($CaCl_2$ or $ZnCl_2$) was injected sequentially into a 1.46 mL titration cell initially containing either acetate buffer or the pectin solution (2.90 mM of Gal). Each injection lasted 20 s, and an interval of 1000 s was considered between successive injections. A rotating 250 μL Hamilton micro syringe ensuring constant stirring of the whole mixed dispersion at a speed of 250 rpm was employed for the homogenization during injection. The heat after each injection is derived by calculating the area under each peak. The total heat content, Q, of the solution contained in V_0 is given by eqn (2):

$$Q = [M]_t \times V_0 \times N \times \Delta H \times \theta \tag{2}$$

where $[M]_t$ is the total amount of the pectin in the cell, N is the number of binding sites per Gal unit, ΔH is the binding enthalpy and θ is the fraction of sites occupied by the ligand $[L]$ (which here refers to Ca or Zn concentration). The binding isotherm obtained by integrating injection peaks could be fitted by a model of independent binding sites (eqn (3)) using a nonlinear least-squares minimization method implemented in the analysis software provided with the calorimeter (Microcal Origin software (v.7.0552)).

$$Q = V_0 \Delta H$$
$$\times \left[[L] + \frac{1 + [M]_t N K_b - \sqrt{\left(1 + [M]_t N K_b - [L] K_b\right)^2 + 4 K_b [L]}}{2 K_b} \right] \tag{3}$$

Iterative curve fitting yielded thermodynamic parameters including the binding constant K_b, binding enthalpy ΔH, and stoichiometry N. A full thermodynamic profile is then obtained using the relationships shown in the following equation (eqn (4)).

$$\Delta G = \Delta H - T \Delta S = -RT \ln(K_b) \tag{4}$$

where ΔG, ΔH and ΔS are the Gibbs free energy, enthalpy and entropy of binding, respectively. T is the absolute temperature and $R = 8.314$ J mol^{-1} K^{-1} is the ideal gas law constant. All the measurements were done at least in triplicate.

Viscosity measurements. We performed viscosity measurements using a capillary viscosimeter (SI analytics, Germany) and measured the flow time. The viscosimeter was immersed in a thermostatic water bath at 30 °C. After loading the sample into the viscosimeter, the solution was allowed to equilibrate at the bath temperature before starting the experiment. All experiments were done at least in triplicate.

Small angle neutron scattering. We performed small angle neutron scattering (SANS) measurements on the PACE spectrometer (Laboratoire Léon Brillouin, CEA-Saclay, Gif-sur-Yvette, France). Three configurations were used with two different neutron wavelengths and two sample detector distances ($\lambda = 13$ Å and $D = 4.7$ m; $\lambda = 5$ Å and $D = 4.7$ m; $\lambda = 5$ Å and $D = 0.9$ m) that cover the 0.0032–0.5 Å^{-1} wave vector range. We applied standard corrections for sample volume, neutron

beam transmission, empty cell signal, and detector efficiency to the raw signal to obtain scattering in absolute units, and then removed the signal from the buffer.[18] All experiments were done in acetate deuterated buffer.

Molecular dynamics simulations. To better understand the way the two divalent cations interact with the Gal units of LMP, we performed molecular dynamics (MD) simulations using the CHARMM program.[19] We first investigated the structure of a pair of octameric Gal chains bridged by four divalent cations (see Fig. 4). The chains were built following an analogous procedure to that described by Braccini and Pérez[12,20] and put in a cubic simulation box of water molecules. Given that the structure of these complexes remained stable over the simulation time scale (20 ns), we then investigated the ability of Ca^{2+} and Zn^{2+} to induce the association of Gal chains. For this purpose, we performed 100 ns long simulations in which (i) the two Gal chains were initially dissociated from each other, and (ii) calcium or zinc cations were initially free (see Fig. S3 in the ESI†). We also run independent simulations of the two divalent cations alone in water to determine their average hydration number in the bulk. Finally, we performed additional umbrella sampling simulations to investigate more specifically the interaction strength of the divalent cations with either the carboxylate group of Gal or with water. All simulations were performed at a temperature of 300 K and chloride or sodium ions were added to the simulation boxes to ensure charge neutrality. Further details on all of these simulations are provided in the ESI.†

Results

Turbidity and viscosity measurements

The turbidity and intrinsic viscosity measurements of pectin solutions as a function of the molar ratio R (= cation/Gal) are presented in Fig. 1. At low molar ratios, turbidities remain constant – at a relatively low value (<0.05 cm^{-1}) – and similar for
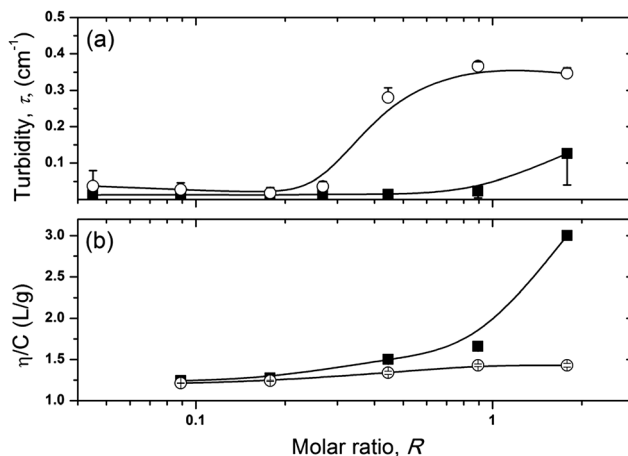

Fig. 1 (a) Evolution of turbidity at 500 nm and (b) intrinsic viscosity normalized by the concentration (η/C) ($T = 30$ °C) as a function of the molar ratio, R, (divalent cation/Gal) for calcium cations (black squares) and zinc cations (empty circles).

both cations (Fig. 1a). At $R = 0.27$, an abrupt increase of turbidity appears for pectin–Zn^{2+} solutions, while only a modest increase of turbidity is noted for pectin–Ca^{2+} solutions, at a much higher molar ratio ($R > 1.00$).

We then measured the intrinsic viscosity of pectin–cation mixtures at different molar ratios (Fig. 1b). At low molar ratios, intrinsic viscosity remains constant with a relatively low value ($\sim$1.25 L g^{-1}) and similar for both cations. Upon addition of calcium, we observe a slight increase of the intrinsic viscosity which accelerates at $R \sim 0.9$. Fang et al.[13] have found similar changes in relative viscosities of LMP solution (0.5 g L^{-1}) upon titration with calcium, but at $R \sim 0.25$. The difference of the inflexion ratio may be due to the type of the studied pectin (molecular weight, ramification, DE,…) and to its concentration (1 g L^{-1} in our study). Besides, the intrinsic viscosity does not change significantly whatever the amount of zinc added in the studied ratio range. The very low increase of viscosity and steep increase of turbidity of the zinc solution are counter-intuitive and suggest that the gel formed is very heterogeneous. Indeed, the strong rise of turbidity probably reveals the formation of large-scale density fluctuations that strongly scatter light. Yet, the slight increase of viscosity implies that such heterogeneous zones interconnect weakly with each other. The opposite trends observed for the gel formed by LMP upon addition of calcium suggest comparatively a more homogeneous structure of the gel at the mesoscopic scale.

Thermodynamic behavior of the cation–pectin complex

The interactions between pectin and various divalent cations may induce a release (exothermic) or an uptake (endothermic) of heat. Thermodynamic measurement obtained by ITC provides quantification of the change in energy when going from the free to the bound state. The binding enthalpy (ΔH) is presented for LMP solution as a function of the nature of divalent cations at various molar ratios (Fig. 2). Both endothermic (at low molar ratios $\leq$0.3) and exothermic (at high molar ratios >0.3) phenomena are observed, thereby suggesting

that the binding mechanism is characterized by at least two processes. The first process is endothermic and may be ascribed to the formation of both monocomplexes between divalent cations and carboxylate groups[13] and of *point-like cross-links* (formation of one Gal–cation–Gal bridge between two Gal chains).[21] The second process is exothermic and corresponds to the formation of an ordered structure that can be attributed to the formation of dimers (or multimers). The existence of these two thermal transitions is in agreement with the findings obtained by several authors.[13,22] For instance, Fang et al. have observed a reduction of binding heat in the first step followed by an increase of binding heat in the second step.[13]

For the first injections of divalent cations slight differences appear between the titration curves of calcium and zinc (Fig. 2). These differences then vanish for higher molar ratios. The thermodynamic parameters determined by fitting the positive part of the curves with a model of independent binding sites using eqn (3) and (4) are summarized in Table 1. The initial portions of the calorimetric titration curves show that the enthalpy of the zinc–LMP complex ($\Delta H = 18.1 \pm 5.6$ kJ mol^{-1}) is higher than the enthalpy of the calcium–LMP complex ($\Delta H = 12.1 \pm 0.3$ kJ mol^{-1}), but the binding sites for both calcium and zinc complexes present similar free energy ($\Delta G \sim -24.6$ kJ mol^{-1}). It may imply an enthalpy–entropy compensation for both calcium and zinc pectin complexes. The binding of cations to Gal groups is entropy driven, since the dehydration of both cations and carboxylate groups leads to a significant entropy gain (release of tightly bound water molecules), which over-balances the unfavorable enthalpy change.[23] We also observe that the site number, N, is higher for calcium than for zinc cations. We can suppose that only a few Gal groups are associated to zinc cations (one cation for $\sim$5 and $\sim$14 units of Gal for calcium and zinc, respectively). Furthermore, the binding enthalpy changes from positive to negative at around $R = 0.25$ and $R = 0.35$ for calcium and zinc, respectively, indicating that at these ratios, the binding process becomes exothermic ($\Delta H < 0$) and corresponds to the second step (dimerization), in line with previous studies.[13,24]
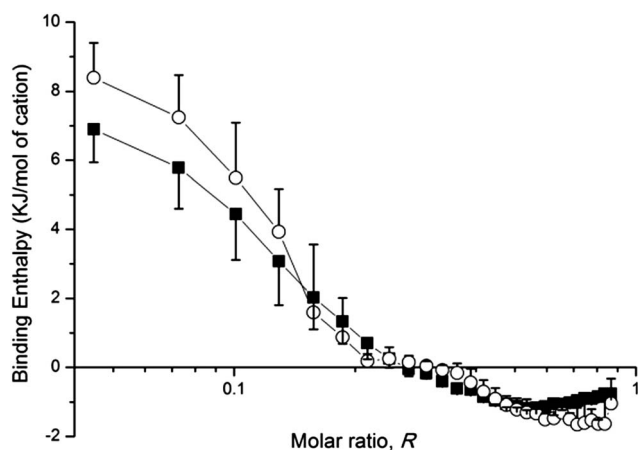
Molecular description of the cation–pectin complex

SANS measurements of pectin with and without divalent cations (Ca^{2+} and Zn^{2+}) allow us to describe the local conformation of pectin in solutions and gels, and to determine the persistence length of the polymer. The SANS scattering intensity for pectin (2.90 mM of Gal) in the presence of calcium and zinc cations was investigated at two molar ratios corresponding to the positive ($R = 0.09$) and the negative ($R = 0.44$) binding enthalpies observed by ITC (Fig. 3).

A transition between a q^{-d}-like decay at low q, with $3 \leq d \leq 4$ (due to the branched structure of pectin and/or to the presence of aggregated regions) and a q^{-1} decay at larger q (rod-like behavior) is found. This transition occurs at q^* ($\sim$0.02 Å^{-1}), which corresponds to the q-limit of the regime for which the scattering exclusively arises from the chain stiffness.[18,25] The persistence length $L_p = 6/(\pi \times q^*)$ characterizes this stiffness and lies in the range of 50–70 Å, depending on the

Fig. 2 Binding enthalpy, ΔH, versus molar ratio, R, obtained from ITC analysis for calcium cations (black squares) and zinc cations (empty circles).

Table 1 Thermodynamic parameters of the first step of divalent cation–LMP interactions at pH 5.3 and at 25 °C determined with the model of independent binding sites from the Microcal origin software. N is the number of binding sites per Gal unit, K_b is the binding constant, ΔH is the binding enthalpy, ΔS is the entropy and ΔG is the free energy

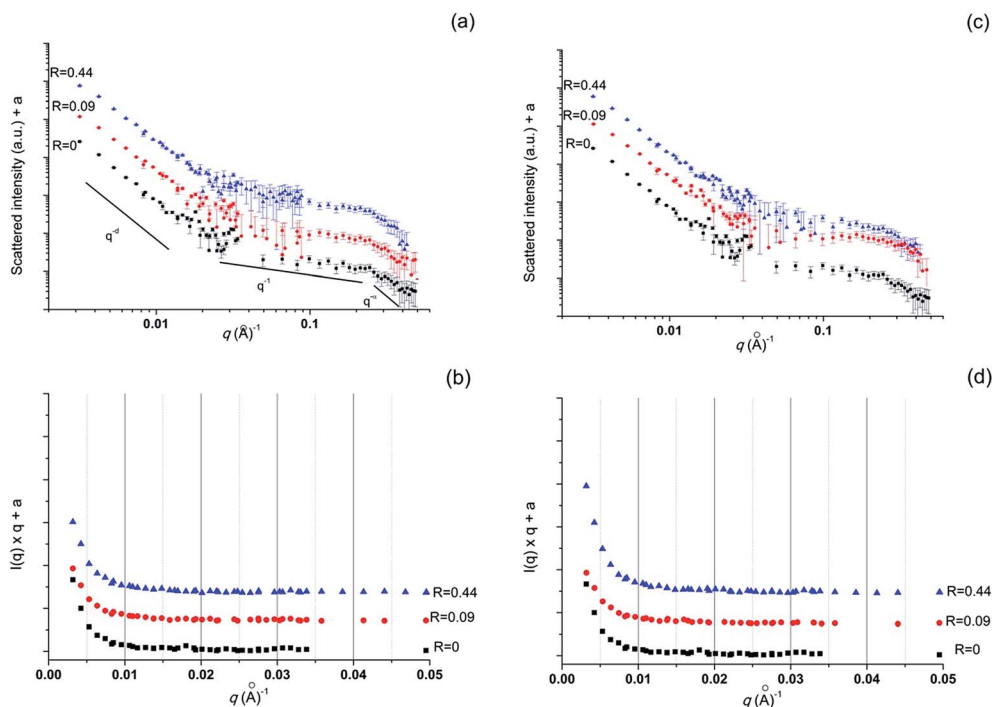|	N	$10^{-3}\,K_b$ (M^{-1})	ΔH (kJ mol^{-1})	$T\Delta S$ (kJ mol^{-1})	ΔG (kJ mol^{-1})
Ca	0.19 ± 0.03	20.5 ± 0.3	12.1 ± 0.3	36.6 ± 0.4	-24.6 ± 0.1
Zn	0.07 ± 0.04	21.5 ± 7.6	18.1 ± 5.6	42.6 ± 4.6	-24.5 ± 0.9

Fig. 3 SANS spectra of pectin solution (2.90 mM of Gal) in the presence of calcium (a) and zinc (c) cations. Graphs (b) and (d) correspond to $I(q) \times q$ versus q for calcium and zinc, respectively. All experiments were done in acetate buffer and at fixed temperature (pH = 5.3, T = 25 °C, respectively).

concentration of pectin. Previous studies have found a q^* value around 0.04 Å^{-1}, which gives a persistence length of the order of 80 Å for pectin (10 g L^{-1}) in 25 mM buffer, corresponding to 16–17 sugar units.[18] We observed a second break of slope around q = 0.2 Å^{-1} that could represent the thickness of monomers (or cross-section). Unfortunately, the large uncertainty arising from the solvent subtraction in this regime does not allow a proper evaluation of such cross-section dimensions. After the introduction of calcium, no significant changes are observed. The intersection between the two regimes q^{-d} and q^{-1} is similar, indicating that the L_p remains constant for the two studied molar ratios. To better evaluate differences in the structure of the pectin in the presence of divalent cations, the scattering intensity is fitted by a squared-Lorentz function according to the Debye–Bueche model (DB) (eqn (5)). Note that this model is applied for $q < q^*$.

$$I(q) = \frac{I_0}{\left(1 + q^2 \Xi^2\right)^2} \quad (5)$$

where I_0 is the zero-q scattering intensity and Ξ is the characteristic length of gel inhomogeneities or two-phase separated structures. It was demonstrated that the scattered intensity is proportional to the product of 3 quantities: (i) squared fluctuation in scattering length density ($\Delta\rho^2$) between the phases, (ii) a volume fraction (ϕ), and (iii) Ξ^3 according to the equation eqn (6):[26]

$$I_0 = 8\pi\phi\Delta\rho^2\Xi^3 \quad (6)$$

The DB model includes a correlation length Ξ that is interpreted as a distance between the network nodes. The Ξ values obtained from the fitted data are around 374 ± 24 Å for pectin alone, and decrease ($\sim$300 Å) when calcium or zinc is added, indicating a collapse of the structure (Table 2). When calcium cations are further added to pectin, no significant changes in the local conformation are observed (Ξ, I_0 and $\phi\Delta\rho^2$ increase moderately when R increases from 0.09 to 0.44). When zinc cations are added, we observe an increase of both Ξ and I_0 for $R = 0.44$, which induces an increase of $\phi\Delta\rho^2$. If we assume that the volume fraction ϕ in the pectin chain is constant in all

Table 2 Ratio R dependence of the characteristic length, Ξ, and I_0 determined by fitting the SANS spectra against eqn (5) ($q < 0.02$ Å^{-1}). $\phi\Delta\rho^2$ is then obtained from eqn (6)

Molar ratio, R	Ξ (Ca) (Å)	Ξ (Zn) (Å)	I_0 (Ca) (cm^{-1})	I_0 (Zn) (cm^{-1})	$\phi\Delta\rho^2$ (Ca)	$\phi\Delta\rho^2$ (Zn)
0	374 ± 24	374 ± 24	14.5 ± 2.8	14.5 ± 2.8	11.0×10^{-9}	11.0×10^{-9}
0.09	301 ± 14	290 ± 15	6.7 ± 0.9	6.2 ± 0.9	9.8×10^{-9}	10.0×10^{-9}
0.44	306 ± 14	329 ± 18	9.5 ± 1.3	16.7 ± 2.7	13.0×10^{-9}	19.0×10^{-9}

mixtures, it can easily be shown that the squared fluctuation in density ($\Delta\rho^2$) is almost 2 times higher for $R = 0.44$ than for the other molar ratio. Since all phases contain at the same time pectin and buffer, this squared fluctuation in density arises from variation of local concentration of pectin. The increase of $\Delta\rho^2$ in the case of high amounts of zinc may be explained by the formation of pectin-rich and pectin-poor domains within the gel. The absence of such local important fluctuations of concentrations in the case of calcium shows that the system is clearly more homogeneous than with zinc.

Molecular dynamics simulations

We then performed MD simulations to try to understand at the atomistic scale how the two divalent cations interact with the Gal units of LMP. Fig. 4 shows the time-averaged structure of the complex formed by two Gal octamers in the antiparallel arrangement in the presence of either Ca^{2+} or Zn^{2+}. Significant differences are found in the way the cations interact with the Gal chains: whereas Ca^{2+} interacts only with carboxylate groups of Gal, Zn^{2+} interacts also with neighboring hydroxyls. The structure formed in the presence of calcium deviates from that previously determined by Braccini and Pérez,[12] and even more from that of the egg-box model, first hypothesized by Grant *et al.*[11] It must be pointed out that in ref. 12 galacturonate or guluronate chains were assumed to be rigid and the water solvent was not considered explicitly. As such, these calculations did not consider any conformational changes that may occur upon chain association and neglected the competition between water and carboxylate groups for binding to divalent cations, which influences their coordination (see results from Fig. 5). Recent molecular dynamics simulations of guluronate chains in explicit water[27,28] actually showed that guluronate chains are twisted. Interestingly, the interaction of Ca^{2+} with carboxylate groups of Gal chains is bidentate, similar to that observed for Ca^{2+} bridging together two guluronate chains,[28] whereas that of Zn^{2+} is monodentate. It must be pointed out that in the egg-box model, four oxygens from two opposite carboxyl and hydroxyl groups strongly interact with calcium in a monodentate coordination. Therefore, our results clearly indicate that only zinc associates in an egg-box-like configuration (Fig. 4c).

To understand why Ca^{2+} and Zn^{2+} differ in their interactions with Gal chains, we determined the potentials of mean force (PMF) for the interaction of these cations with either water or with a Gal monomer by means of umbrella sampling simulations (see the Molecular dynamics simulation section in the ESI†). A PMF describes the change in the free energy of the
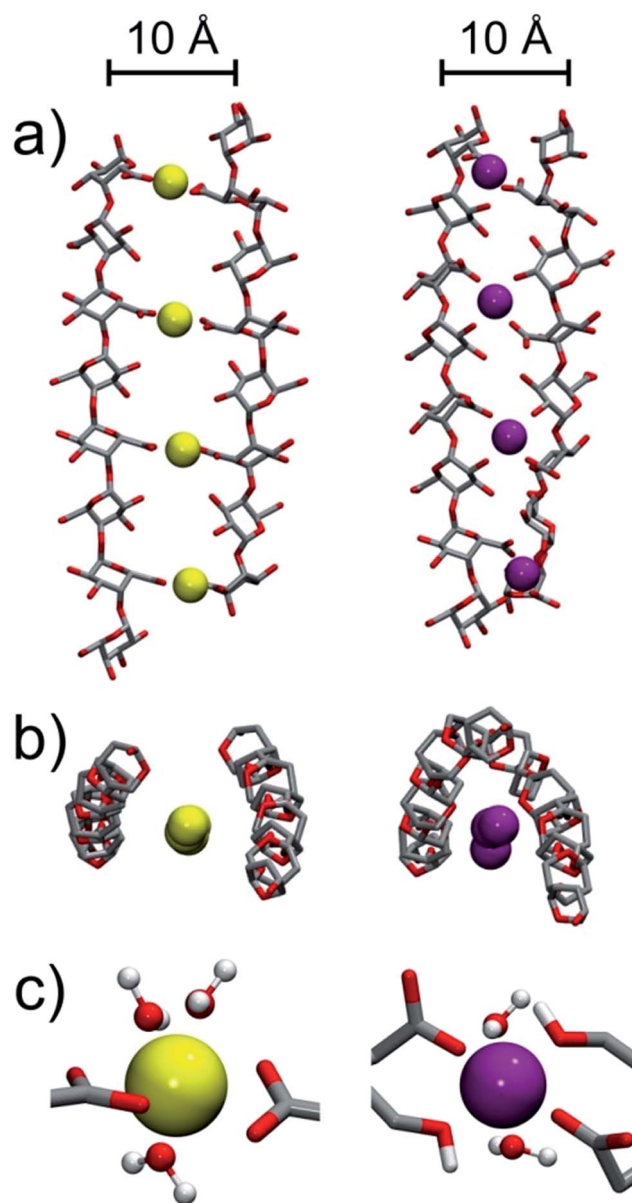

Fig. 4 Time-averaged structures formed by two Gal chains in the antiparallel arrangement in the presence of either calcium (left panels) or zinc (right panels) cations: (a) side view and (b) top view. (c) Examples of configurations of calcium and zinc interacting with Gal chains. For clarity, the atoms shown correspond to heavy atoms in (a), to heavy ring atoms in (b), and to the closest atoms from the divalent cations in (c). Furthermore, water molecules in the first hydration shell of the two divalent cations are also represented in (c).

system as a function of a reaction coordinate. It is thus very useful to determine free energy barriers and minima between two interacting species (either cation and water or cation and Gal in our study). The PMFs for the interaction between cations and water (Fig. 5a) exhibit two minima that correspond to water molecules located in the first and second hydration shells of the cations, respectively. These minima are found at shorter distances for Zn^{2+} (2.1 and 4.3 Å) than for Ca^{2+} (2.3 and 4.6 Å), consistent with the smaller size, higher charge density and stronger affinity for water of Zn^{2+} with respect to Ca^{2+}. The energy barrier to exchange a water molecule from the 1st to the 2nd solvation shell is much larger for Zn^{2+} (34 kJ mol^{-1}) than for Ca^{2+} (about 15 kJ mol^{-1}), which suggests that the kinetics for desolvating Zn^{2+} is much slower than that for Ca^{2+}. The PMFs for the interaction of the divalent cations with a Gal monomer exhibit three main features (Fig. 5b): (i) two deep minima close to each other, at distances ranging from 2.5 to 3.3 Å, (ii) an

energy barrier at distances close to 3.7 and 4.0 Å, and (iii) a relatively shallow and broad minimum at distances between 4.5 and 5.5 Å. The two deep minima correspond to configurations where the cations are in contact with either one (monodentate coordination) or two oxygens from the carboxylate group of Gal (bidentate coordination). Interestingly, the global minimum of the PMF for Ca^{2+} (at $r = 2.5$ Å) corresponds to a bidentate coordination with the carboxylate group (minimum (1) in the inset of Fig. 5b), whereas that for Zn^{2+} (at $r = 3.2$ Å) corresponds to a monodentate one (minimum (2) in the inset of Fig. 5b). This result appears consistent with the MD study of Iskrenova-Tchoukova *et al.*,[29] who found that the interactions of Mg^{2+} and Ca^{2+} with a carboxylate group are preferentially monodentate and bidentate, respectively. These authors ascribed the monodentate coordination of Mg^{2+} to its strong interaction with water, which makes unlikely the loss of an additional first-shell water molecule for binding to the other carboxylate oxygen. This reason probably holds true when comparing Zn^{2+} and Ca^{2+}, since Zn^{2+} interacts much more strongly with water than Ca^{2+} does, given its smaller radius. Besides, the free energy barriers at distances close to 3.5 Å separate the contact ion pair (CIP) configurations from the solvent separated ion pair (SSIP) ones, where the carboxylate group and the divalent cations share with each other their hydration shells (see Fig. S2 in the ESI†). The corresponding energy barrier is remarkably larger for zinc than for calcium (about 16 kJ mol^{-1} *vs.* 8 kJ mol^{-1}), in line with the larger free energy barrier to exchange water between the 1st and the 2nd hydration shells of zinc (Fig. 5a). Accordingly, the PMFs in Fig. 5b suggest that binding to the carboxylate groups of Gal chains takes longer for zinc than for calcium. Moreover, the free energy difference between the global minimum (the most stable CIP) and the free state for cation–carboxylate association is significantly more favorable for zinc than for calcium (about 53 kJ mol^{-1} *vs.* 41 kJ mol^{-1}). Both the strong cation–Gal interaction observed for Zn^{2+} and its monodentate coordination – which induces an egg-box-like configuration – explain why the Gal chains stay closer to each other than in the presence of Ca^{2+} (Fig. 4).

We then calculated the averaged numbers of water molecules found in the first shell of the divalent cations as a function of their distances from the carboxylate group of Gal (Fig. 5c). At distances $r > 6$ Å, these numbers are close to 7.2 and 6.0 for Ca^{2+} and Zn^{2+}, respectively, in line with those that we determined from complementary MD simulations of the cations in the bulk (7.22 ± 0.44 and 6.00 ± 0.01). They also lie in the range of coordination numbers reported in the literature from numerous experimental and computational studies (6.2–9 for Ca^{2+} and ≈ 6 for Zn^{2+}, see, *e.g.* ref. 30 and 31 and references therein). The behaviors of the coordination numbers of Ca^{2+} and Zn^{2+} are strikingly different when these cations approach closer and closer from the carboxylate group of Gal. The coordination number of Ca^{2+} steeply decreases upon binding to the carboxylate group of Gal, so that Ca^{2+} loses on average about 1.5 and 2.1 water molecules in the monodentate and bidentate coordinations, respectively. In contrast, the coordination number of Zn^{2+} decreases to ~5 when Zn^{2+} binds to Gal in the monodentate and bidentate coordinations. Such different
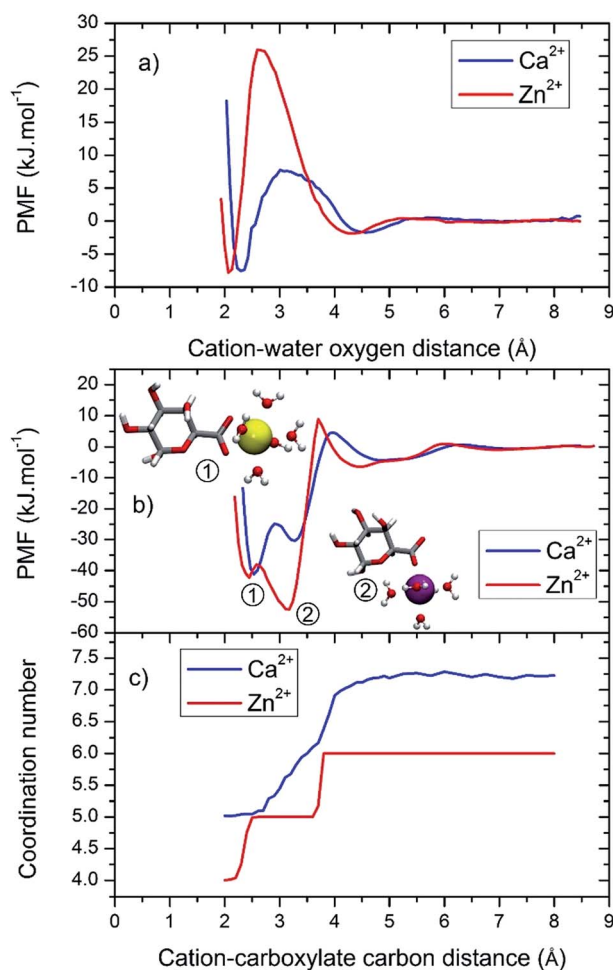

Fig. 5 Potentials of mean force (PMFs) for the interaction between the divalent cations and either (a) water or (b) Gal. The global minima (1) and (2) – inset pictures in (b) – correspond to configurations where Ca^{2+} and Zn^{2+} are in contact with the carboxylate group of Gal in the bidentate or the monodentate coordination, respectively. The average numbers of water molecules in the first hydration shell of Ca^{2+} and Zn^{2+} as a function of their distances from the carboxylate group of Gal are shown in (c).

behaviors probably originate from the differences found in the free energy barriers that water molecules from the 1st hydration shell of the cations need to cross to exchange with 2nd shell water molecules (Fig. 5a). This water exchange process is obviously much more unlikely for water hydrating Zn^{2+} than for those hydrating Ca^{2+}, as reflected by the much lower standard deviation for the coordination number of Zn^{2+} in comparison with that of Ca^{2+} found for these cations in the bulk (0.01 *vs.* 0.44).

We then investigated the ability of Ca^{2+} and Zn^{2+} to induce the association of Gal chains. For this purpose, we performed simulations in which (i) the two Gal chains were initially dissociated from each others, and (ii) calcium or zinc cations were initially not bound to the Gal chains (see Fig. S3 in the ESI†). We determined the number of contacts formed between the cations and carboxylate groups to describe the binding process (Fig. 6). A cation–Gal contact was considered to exist if the distance between the cation and the C6 atom of Gal residues (see Fig. S1 in the ESI† for atom names) was lower than 3.65 Å. This distance criterion was established from the C6–cation pair radial distribution functions (data not shown) and corresponds to distances shorter than the distances of the desolvation free energy barriers in Fig. 5b. The simulations show that the binding of Ca^{2+} cations to Gal (monocomplexation) occurs in the 1–5 ns time range, whereas that of Zn^{2+} lies in the 4–42 ns range. The much longer times found for Zn^{2+} are fully consistent with the larger free energy barrier in the PMF for the interaction of Zn^{2+} with the Gal monomer (Fig. 5b).

Furthermore, within the time scale of these simulations ($t = 100$ ns), no association of the two Gal chains is observed in the presence of Zn^{2+} ($N_c = 4$ corresponds to the monocomplexation of each cation with the Gal chains), whereas Ca^{2+} cations induce the formation of two bridges between the two Gal chains at simulation times of about 30 and 50 ns ($N_c = 6$ indicates that the 4 cations are complexed with Gal and that two Gal–cation–Gal cross-links are formed). Fig. 6 also reveals that the monocomplexation process occurs before the formation of cross-links and thus before dimerization. In addition, these simulations clearly suggest that the formation of point-like cross-links between Gal chains enables the formation of a stable three-dimensional network.

Discussion

In the absence of divalent cations, the low-q-dependence of SANS spectra is much larger than that expected for a chain with a self-avoiding behavior ($I(q) \propto q^{-1.7}$), thereby indicating that LMP chains show signs of self-association (Fig. 3). This may stem from (i) inter- and/or intramolecular hydrogen bonds between hydroxyl and/or carboxylate groups of pectin, or from (ii) hydrophobic association between methyl groups of methyl-esterified α-D-galacturonic or rhamnose residues for instance. The association between chains is probably rather loose and highly fluctuating, since (i) the hairy regions of pectin prevent an efficient packing between adjacent chains for straightforward steric reasons, and (ii) the interaction between the carboxylate groups of neighbouring Gal residues is not favorable owing to their electrostatic repulsion. To better illustrate this, schematic representations of the structure formed by LMP in either the absence or in the presence of the zinc and calcium cations that can be deduced from our results are shown in Fig. 7.
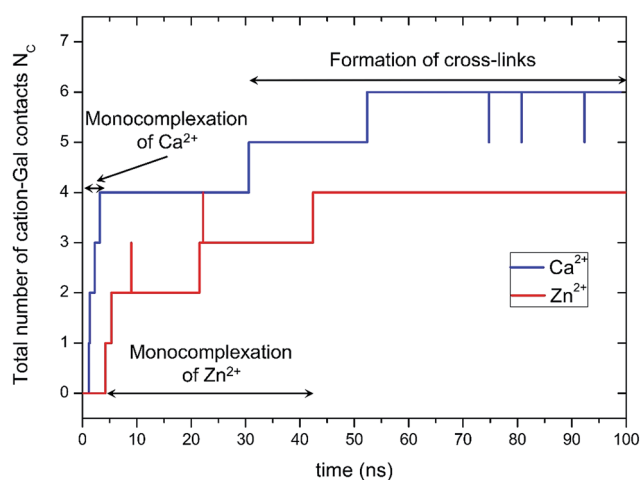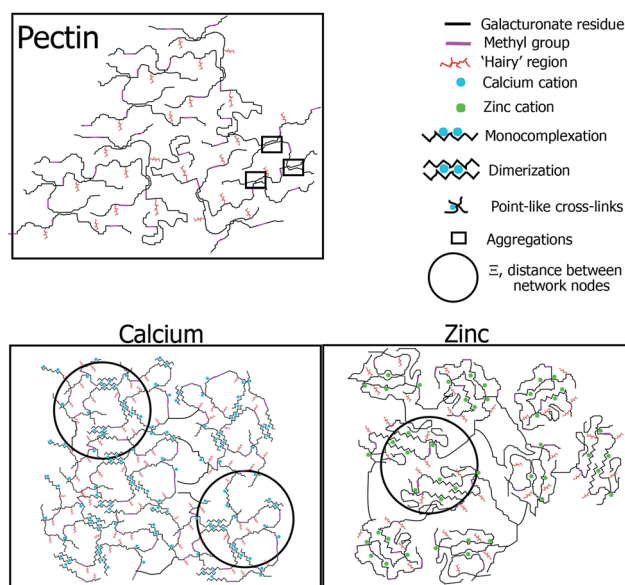

Fig. 6 Time evolution of the total number of contacts formed between the divalent cations and the carboxylate groups of the Gal chains, N_c. A contact was considered to be formed if the distance between the cations and the C6 atom of Gal units was lower than 3.65 Å. Any cation–Gal complexation increases N_c by 1. Accordingly, a Gal–cation–Gal bridge accounts for two contacts. In the initial configuration ($t = 0$ ns), the two Gal chains are dissociated and none of the divalent cations is in contact with them ($N_c = 0$). In the final configuration ($t = 100$ ns), the monocomplexation of both Ca^{2+} and Zn^{2+} is completed (that is, each cation is in contact with Gal), but only Ca^{2+} has induced the association of the two Gal chains (formation of cross-links). Fig. S3, Movies S1 and S2† on these simulations are provided in the ESI.†

Fig. 7 Suggested scheme for the network of calcium and zinc pectin complexes at $R = 0$ (pectin alone) and $R = 0.44$.

At low molar ratios ($R < 0.25$), the binding enthalpy determined in ITC experiments is endothermic indicating that the binding between divalent cations and LMP is entropically driven. For the first cation injections, the binding enthalpy is higher for zinc ($\Delta H = 18.1$ kJ mol^{-1}) than for calcium ($\Delta H = 12.1$ kJ mol^{-1}). Thus, the binding of zinc to carboxylate groups of Gal is more difficult than the binding of calcium. This is in agreement with the larger free energy desolvation barrier of zinc compared to calcium found in our MD simulations (Fig. 5a), which show that water molecules hydrating zinc are less exchangeable than those hydrating calcium. Moreover, we observed an abrupt decrease of the gel's Ξ from 374 Å to respectively 301 Å for calcium and 290 Å for zinc when the ratio R increases from 0 to 0.09, showing a reduction of the distance between the network nodes. Since the decrease of the correlation length Ξ cannot arise from the formation of monocomplexes, it necessarily stems from (i) the formation of point-like cross-links between neighbouring chains, in agreement with Ventura *et al.*,[21] (ii) and/or from the formation of dimers and multimers (Fig. 7). In other words, the SANS data show that both monocomplexes and point-like cross-links already coexist at low molar ratios. This is consistent with the rather strong binding of divalent cations to Gal found in the MD simulations, which makes likely the formation of Gal–cation–Gal bridges already at low molar ratios. Our findings suggest that the partial monocomplexation of pectin is sufficient to form a network connected by stable point-like cross-links.

At intermediate and high molar ratios ($R > 0.25$), pectin chains become closer to each other, forming an ordered structure which corresponds to the exothermic process observed in ITC. This process was assigned to the dimerization step (association between two chains bridged by cations) observed by several authors.[13,21,22,32] According to SANS findings, Ξ lengths are similar for both $R = 0.09$ and $R = 0.44$ ($\Xi \sim 300$ Å) when calcium was added. The local structure (Table 2) and the macroscopic behavior (Fig. 1b) of the LMP–Ca did not change significantly, meaning that the dimerization may occur at the same time as the formation of monocomplexes and junction zones. This is in line with Fang *et al.*, who concluded that in contrast to alginate, the dimerization of LMP with calcium emerges immediately upon addition of calcium even if the stoichiometry ($R = 0.25$) is not satisfied.[13] They have shown that this dimerization consists mainly in the formation of point-like cross-links, which can be explained by the blockwise and random distribution of ester groups present in pectin that prevent the formation of long sequences of pectin–calcium–pectin bridges.

When zinc cations are added, a small increase of the Ξ length ($\sim$329 Å) accompanied by a twofold increase of the squared fluctuation in density ($\Delta\rho^2$) are observed for $R = 0.44$, showing the formation of large concentration fluctuations within the gel. The typical sizes of these density fluctuations are large enough to scatter light, explaining the increase of the turbidity observed for LMP–Zn (Fig. 1a) at such R. This indicates that aggregation and local shrinkage may occur. Indeed, it is important to remember that the forces that cause aggregation, *e.g.* local charge neutralization of carboxylate groups by adding cations, will often also be accompanied by shrinkage of the same aggregates.[33] Jonassen *et al.* have recently studied by dynamic light scattering and turbidity measurements the interaction between LMP and zinc cations.[34] They supposed that the addition of zinc cations induces the formation of a semi-cross-linked polymer network. The formation of such aggregates in the presence of zinc makes the distribution of pectin in the solution very heterogeneous and reduces its ability to form a percolating network. It has thus a minor influence on the macroscopic viscosity, as observed in Fig. 1b. As a consequence, the average overlap between chains (interactions between distinct aggregates) decreases. In contrast to zinc, the turbidity of calcium–LMP solutions increases slowly when the calcium cation is added indicating the progressive formation of aggregates. The low increase of turbidity may be also due to the presence of both aggregates (large objects with refractive index distinct from that of the medium) and to the formation of a continuous network (larger and less compact objects that have a refractive index closer to that of the medium), as confirmed by SANS measurements (Table 2). The formation of this continuous network can explain the steady increase of intrinsic viscosity observed at $R > 0.9$ (Fig. 1b). MD simulation of two Gal chains in the presence of divalent cations (Fig. S3, Movies S1 and S2 in the ESI†) confirms these observations. Indeed, at a given simulation time ($t = 100$ ns), both calcium and zinc were bound to the Gal chains (Fig. S3b in the ESI†). However, calcium induces the association of the two Gal chains, which can be considered as a precursor of a percolating network, while the two Gal chains remain dissociated in the presence of zinc. This may be explained by the mode of interaction between calcium and Gal (Fig. 4a): the bidentate coordination makes the association of Gal chains looser and also improves their ability to associate with each other, not only by dimerization, but also by the formation of point-like cross-links. Conversely, the mode of interaction between zinc and Gal, which looks closer to the egg-box model (monodentate coordination and tighter association of Gal chains, Fig. 4a), reduces the number of topological ways in which chains may associate with each other. For instance, chains should probably be more aligned with each other in the presence of zinc than in the presence of calcium for association to occur.

Conclusion

In this study, we investigated the interactions between low methoxy pectin and either Ca^{2+} or Zn^{2+} in semi-dilute solutions at different scales in association with MD simulation. Our results show that the addition of divalent cations changes the structure and the organization of LMP chains in several ways. The strong binding of cations to the carboxylate groups of Gal residues (monocomplexation) favors the formation of cross-links and/or the dimerization (or multimerization) of adjacent chains *via* bridges between neighbouring carboxylate groups. These associations of adjacent chains reduce the average distance between the nodes of the network formed (as indicated by the characteristic length Ξ determined from SANS measurements). In addition, our results suggest that the

network of pectin chains formed in the presence of Ca^{2+} is more homogeneous than the one formed in the presence of Zn^{2+}. The difference in this structure can be attributed to the way the cations interact with Gal. Indeed, MD simulations evidenced that the dehydration of zinc is more difficult than that of calcium. They also showed that zinc interacts with both carboxylate and hydroxyl groups of Gal, in a similar way to that described in the egg-box model, whereas calcium only interacts with carboxylate groups. These two different modes of interaction induce very different mobilities of chains; thus, calcium pectin seems to be more flexible than zinc pectin. This may explain why dosage forms prepared with calcium pectinate are more sensitive to water uptake than those made up with zinc, as observed previously,[14,16] and thus, why drug release is much faster in the case of calcium pectinate forms.

Conflict of interest

The authors declare no competing financial interest.

Acknowledgements

References

1 P. Cescutti and R. Rizzo, *J. Agric. Food Chem.*, 2001, **49**, 3262–3267.

2 V. M. Dronnet, M. A. V. Axelos, C. M. G. C. Renard and J.-F. Thibault, *Carbohydr. Polym.*, 1998, **35**, 29–37.

3 D. Thom, G. T. Grant, E. R. Morris and D. A. Rees, *Carbohydr. Res.*, 1982, **100**, 29–42.

4 M. Torre, A. R. Rodriguez and F. Saura-Calixto, *Food Chem.*, 1995, **54**, 23–31.

5 L. Liu, M. L. Fishman, J. Kost and K. B. Hicks, *Biomaterials*, 2003, **24**, 3333–3343.

6 A. G. J. Voragen, W. Pilnik, J.-F. Thibault, M. A. V. Axelos and C. M. G. C. Renard, *Food Polysaccharides and Their Applications*, Taylor & Francis, New York, 1995, 354–397.

7 A.-L. Kjøniksen, M. Hiorth and B. Nyström, *Eur. Polym. J.*, 2004, **40**, 2427–2435.

8 F. Liners and P. Van Cutsem, *Micron Microsc. Acta*, 1991, **22**, 265–266.

9 G. A. Luzio and R. G. Cameron, *Carbohydr. Polym.*, 2008, **71**, 300–309.

10 D. A. Powell, E. R. Morris, M. J. Gidley and D. A. Rees, *J. Mol. Biol.*, 1982, **155**, 517–531.

11 G. T. Grant, E. R. Morris, D. A. Rees, P. J. C. Smith and D. Thom, *FEBS Lett.*, 1973, **32**, 195–198.

12 I. Braccini and S. Pérez, *Biomacromolecules*, 2001, **2**, 1089–1096.

13 Y. Fang, S. Al-Assaf, G. O. Phillips, K. Nishinari, T. Funami and P. A. Williams, *Carbohydr. Polym.*, 2008, **72**, 334–341.

14 A. Assifaoui, O. Chambin and P. Cayot, *Carbohydr. Polym.*, 2011, **85**, 388–393.

15 C. Dhalleine, A. Assifaoui, B. Moulari, Y. Pellequer, P. Cayot, A. Lamprecht and O. Chambin, *Int. J. Pharm.*, 2011, **414**, 28–34.

16 A. Assifaoui, C. Loupiac, O. Chambin and P. Cayot, *Carbohydr. Res.*, 2010, **345**, 929–933.

17 B. M. Yapo, *Food Res. Int.*, 2009, **42**, 1197–1202.

18 I. Schmidt, F. Cousin, C. Huchon, F. Boué and M. A. V. Axelos, *Biomacromolecules*, 2009, **10**, 1346–1357.

19 B. R. Brooks, C. L. Brooks, A. D. Mackerell, L. Nilsson, R. J. Petrella, B. Roux, Y. Won, G. Archontis, C. Bartels, S. Boresch, A. Caflisch, L. Caves, Q. Cui, A. R. Dinner, M. Feig, S. Fischer, J. Gao, M. Hodoscek, W. Im, K. Kuczera, T. Lazaridis, J. Ma, V. Ovchinnikov, E. Paci, R. W. Pastor, C. B. Post, J. Z. Pu, M. Schaefer, B. Tidor, R. M. Venable, H. L. Woodcock, X. Wu, W. Yang, D. M. York and M. Karplus, *J. Comput. Chem.*, 2009, **30**, 1545–1614.

20 I. Braccini, R. P. Grasso and S. Pérez, *Carbohydr. Res.*, 1999, **317**, 119–130.

21 I. Ventura, J. Jammal and H. Bianco-Peled, *Carbohydr. Polym.*, 2013, **97**, 650–658.

22 C. K. Siew, P. A. Williams and N. W. G. Young, *Biomacromolecules*, 2005, **6**, 963–969.

23 L. Ge, M. Vernon, S. Simon, Y. Maham, J. Sjöblom and Z. Xu, *Colloids Surf., A*, 2012, **396**, 238–245.

24 Y. Fang, S. Al-Assaf, G. O. Phillips, K. Nishinari, T. Funami, P. A. Williams and L. Li, *J. Phys. Chem. B*, 2007, **111**, 2456–2462.

25 F. Muller, S. Manet, B. Jean, G. Chambat, F. Boué, L. Heux and F. Cousin, *Biomacromolecules*, 2011, **12**, 3330–3336.

26 P. Debye and A. M. Bueche, *J. Appl. Phys.*, 1949, **20**, 518–525.

27 W. Plazinski, *J. Comput. Chem.*, 2011, **32**, 2988–2995.

28 A. Wolnik, L. Albertin, L. Charlier and K. Mazeau, *Biopolymers*, 2013, **99**, 562–571.

29 E. Iskrenova-Tchoukova, A. G. Kalinichev and R. J. Kirkpatrick, *Langmuir*, 2010, **26**, 15909–15919.

30 J.-P. Piquemal, L. Perera, G. A. Cisneros, P. Ren, L. G. Pedersen and T. A. Darden, *J. Chem. Phys.*, 2006, **125**, 054511.

31 J. C. Wu, J.-P. Piquemal, R. Chaudret, P. Reinhardt and P. Ren, *J. Chem. Theory Comput.*, 2010, **6**, 2059–2070.

32 I. Donati, S. Holtan, Y. A. Morch, M. Borgogna, M. Dentini and G. Skjak-Brak, *Biomacromolecules*, 2005, **6**, 1031–1040.

33 L. T. T. Trinh, H. M. L. Lambermont-Thijs, U. S. Schubert, R. Hoogenboom and A.-L. Kjøniksen, *Macromolecules*, 2012, **45**, 4337–4345.

34 H. Jonassen, A. Treves, A.-L. Kjøniksen, G. Smistad and M. Hiorth, *Biomacromolecules*, 2013, **14**, 3523–3531.